NASA TECHNICAL NOTE

NASA TN D-2360

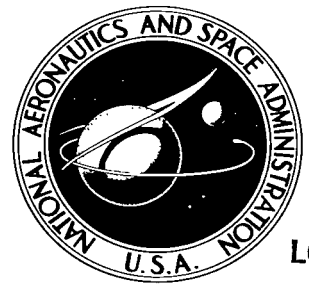

NASA TN D-2360

EFFECTS OF LEADING-EDGE SWEEP ON FLUTTER CHARACTERISTICS OF SOME DELTA-PLANFORM SURFACES AT A MACH NUMBER OF 15.4

by Robert C. Goetz

Langley Research Center
Langley Station, Hampton, Va.

NATIONAL AERONAUTICS AND SPACE ADMINISTRATION • WASHINGTON, D. C. • JULY 1964

ERRATA

NASA Technical Note D-2360

EFFECTS OF LEADING-EDGE SWEEP ON FLUTTER CHARACTERISTICS OF SOME DELTA-PLANFORM SURFACES AT A MACH NUMBER OF 15.4

C.1

By Robert C. Goetz
July 1964

Page 3:

Line 11: Change definition of w to read as follows:

w normal component of velocity (positive in direction of the outward normal), ft/sec

Line 12: In the definition of x, delete word "root" before "leading edge."

Line 13: In the definition of $\bar{x}_0$, delete the word "root" before both the word "leading edge" and the word "chord."

Line 17 and following lines: Insert the following symbols and definitions before the symbols $\bar{x}_{cg}$ and $\bar{y}_{cg}$, respectively:

x_0 pitch axis location measured from leading edge, in.

y coordinate measured in spanwise direction, in.

Page 5:

Line 7: Revise part of sentence following semicolon to read "all profile shapes parallel to the free-stream direction had a 5-percent . . ."

Last line: Change "wing tip" to "wing leading edge."

Page 6, line 6: Change the phrase "All the distributions" to read "Only the mass distributions."

Page 7: In equation (1), add $\mp$ ahead of $\frac{dz}{dx}$; change $\bar{x}_0$ to x_0.
In line 12, change "negative" to "lower."

Page 8: In equation (5), omit sign $\pm$ before brackets; change $\bar{x}_0$ to x_0.
In line 14, add "using average profile shapes of streamwise strips." to end of sentence.

4 Oct 66

Page 9, last paragraph: It has been found that the application of the Newtonian theory to the slab series of airfoils is contrary to some of the assumptions stated. Consequently, the remarks concerning the Newtonian theory calculations of figures 10(c) and 11(c) for the slab series of airfoils as well as the Newtonian theory data appearing in these figures (pp. 33 and 36) should be disregarded.

Page 12: In equation (A4b), change $\bar{x}_0$ to x_0.

Page 13: In equations (A5) and (A6), change $\bar{x}_0$ to x_0.

Page 14: In equations on lines 2, 4, 5, and 6, change $\bar{x}_0$ to x_0.

Page 17: In bracketed headnote under "Overall properties," change $\left[\bar{x}_0 = 0.65\right]$ to $\left[\left(\bar{x}_0\right)_{root} = 0.65\right]$.

Page 21: In the final column of table III, all quantities x/l should be y/s.

Issued 9-12-66

EFFECTS OF LEADING-EDGE SWEEP ON FLUTTER CHARACTERISTICS OF SOME DELTA-PLANFORM SURFACES AT A MACH NUMBER OF 15.4

By Robert C. Goetz

Langley Research Center
Langley Station, Hampton, Va.

NATIONAL AERONAUTICS AND SPACE ADMINISTRATION

For sale by the Office of Technical Services, Department of Commerce,
Washington, D.C. 20230 -- Price $1.00

EFFECTS OF LEADING-EDGE SWEEP ON FLUTTER CHARACTERISTICS OF SOME DELTA-PLANFORM SURFACES AT A MACH NUMBER OF 15.4

By Robert C. Goetz
Langley Research Center

SUMMARY

A wind-tunnel investigation has been conducted in helium flow at a Mach number of 15.4 to determine some effects of leading-edge sweep and profile shape on the flutter characteristics of some delta-planform all-movable control surfaces. The profile shapes tested were blunt leading-edge wedges, double wedges, and slabs. In general, the results indicate that increasing the leading-edge-sweep angle from 60° to about 65° or 70° is destabilizing, while further increases in sweep are stabilizing. However, these trends may be influenced by the layer of disturbed flow along the reflection plane surface, particularly for the more highly swept models. For each sweep angle the blunt double-wedge airfoils are the most susceptible to flutter, and the slab airfoils are the least susceptible to flutter.

Results of flutter calculations made by using modified Newtonian theory and by piston theory aerodynamics in conjunction with an uncoupled two-mode strip analysis are compared with the experimental results. For all cases the Newtonian theory more closely predicted the experimental flutter speeds, particularly for the airfoils with large leading-edge radii.

INTRODUCTION

Highly swept delta planforms with blunt leading edges are extensively used in order to alleviate aerodynamic-heating problems on the lifting surfaces of hypersonic aircraft, missiles, and antimissile missiles. Since many of these vehicles must be capable of operating at relatively high dynamic pressures, the possibility of flutter and other aeroelastic problems must be considered. At present, however, little information is available with regard to the hypersonic-flutter characteristics of such surfaces.

Reference 1 presents a limited amount of theoretical and experimental flutter data for several blunt, highly swept delta surfaces at a Mach number of 7.0. It is the purpose of this report to extend the study of reference 1 to a Mach number of 15.4. Accordingly, a wind-tunnel investigation has been conducted in order to determine some effects of leading-edge-sweep angles and airfoil shapes on the flutter characteristics of several blunt highly swept all-movable control

surfaces at a Mach number of 15.4. These surfaces had leading-edge-sweep angles which varied systematically from 60° to 80°; and all had 5-percent-thick blunted-wedge, double-wedge, or slab airfoils. The experimental results of this investigation are compared with flutter characteristics calculated by second-order piston theory and by modified Newtonian theory.

SYMBOLS

a	speed of sound, ft/sec
b	local wing semichord, ft
b_r	wing root semichord, ft
C_p	normal-pressure coefficient, nondimensional
d	model mounting-shaft thickness, in.
f_n	natural frequency of nth mode (n = 1, 2, 3, and 4), cps
$h(t)$	vertical displacement of elastic axis
I_α	mass moment of inertia of wing about pitch axis, slugs-ft^2
I_{ea}	mass moment of inertia of wing section about pitch axis, lb-in-sec^2
k_r	reference reduced frequency, $\frac{\omega b_r}{V}$
l	model mounting-shaft length, in.
L	lift, lb
L_i	dimensionless coefficient defining lift on an oscillating wing (i = 1, 2, 3, and 4) (See eq. (A7).)
m	mass, slugs
M	Mach number
M_α	total aerodynamic moment on wing about pitch axis, slug-ft
M_i	dimensionless coefficients defining moments on an oscillating wing (i = 1, 2, 3, and 4) (See eq. (A8).)
p_∞	free-stream static pressure, lb/sq ft

Δp local pressure difference between upper and lower wing surfaces, lb/sq ft

R Reynolds number, $\frac{\rho V b_r}{\eta}$

r radius of leading edge, ft

$\bar{r}$ radius of leading edge, fraction of chord

r_α normalized radius of gyration of model about pitch axis, $\sqrt{\frac{I_\alpha}{m b_r^2}}$

s wing semispan, ft

S_α static unbalance about pitch axis, in-lb

t time

V free-stream velocity, ft/sec

w ~~vertical~~ normal component of velocity (positive ~~up~~ in direction of the outward normal), ft/sec

x chordwise coordinate measured parallel to the root chord from the ~~root~~ leading edge, in.

$\bar{x}_0$ pitch-axis location measured from the ~~root~~ leading edge, fraction of ~~root~~ chord

x_0 pitch axis location measured from leading edge, in.

$\bar{x}_{cg}$ streamwise distance from root leading edge to center of gravity of wing, percent of root chord

y coordinate measured in spanwise direction, in.

$\bar{y}_{cg}$ distance from root chord to center of gravity of wing, percent semispan

z coordinate measured perpendicular to chord plane, in.

Z_N function defined by airfoil shape (See appendix.)

$\alpha(t)$ angular perturbation of wing about mean angle-of-attack position

α_0 mean angle of attack, deg

γ ratio of specific heat, 5/3 for helium

η absolute viscosity, slugs/ft-sec

δ spanwise width of model strip, in.

Λ leading-edge-sweep angle, deg

μ mass ratio (ratio of mass of model to mass of volume of test medium contained in cone generated by revolving each chord about its midpoint; height of cone is equal to wing semispan), $\frac{m}{\frac{1}{3}\pi b_r^2 \rho_s}$

ρ density of test medium, slugs/cu ft

ϕ angle between the free-stream direction and a tangent to a point on the wing surface for steady flow, deg

θ local downwash angle caused by unsteady motion

ω frequency of harmonic oscillation, radians/sec

ω_f flutter frequency, radians/sec

ω_n natural frequency of nth mode (n = 1, 2), radians/sec

ω_h frequency of uncoupled first bending mode, radians/sec

ω_α frequency of uncoupled first pitching mode, radians/sec

Subscripts:

ex experimental

stag stagnation

th theoretical

l lower surface

u upper surface

LE leading edge

TE trailing edge

Dot over quantity denotes differentiation with respect to time.

MODELS

Description

The models used in this investigation consisted of three series of half-span all-movable delta surfaces which had leading-edge-sweep angles ranging from 60° to 80° in 5° increments. For each value of sweep angle, three airfoil profile shapes were tested. These were blunt leading-edge wedges, double wedges, and slabs (constant thickness to chord ratio); all shapes had a 5-percent maximum thickness-to-chord ratio and leading-edge radii of 1.25, 1.25, and 2.50 percent of their local chord, respectively. The pitch-axis location of all the models was at 65 percent of the root chord. A sketch showing the model profiles is presented in figure 1, and figure 2 shows a photograph of one series of models with various leading-edge-sweep angles.

The models were supported by a rectangular shaft which was an integral part of the aluminum-alloy core of the model. Bonded to the core was a layer of aluminum alloy covering the inboard portion of the planform; balsa wood covered the remainder of the model; both were machined to give the desired airfoil shape. The aluminum-alloy portion was employed in order to minimize the spanwise center-of-gravity shift with change in leading-edge-sweep angle. Lead inserts were added to the core of the model in order to match closely the mass and inertial properties of the models of reference 1, and to hold a relatively constant frequency ratio (f_1/f_2) for the various models. A photograph of a typical model with the balsa wood removed is shown in figure 3.

Physical Properties

The total mass, inertial parameters, and natural frequencies of the models are listed in table I(a) along with pertinent dimensions. The mass of the model shaft is not included in the data shown.

All models were vibrated with an interrupter air-jet shaker to determine the natural frequencies and nodal patterns. Typical nodal patterns for the models are shown in figure 4. In all cases examined, the third and fourth natural frequencies were well above the first and second natural frequencies. Mode shapes were determined as in reference 2 by taking time-exposure photographs of the models while they were vibrating in one of their first two natural modes. The mode-shape deflections obtained from the photographs showed that within reading error, all elastic deformation of the first two natural modes was confined to the model shaft. Thus, in these two modes, the wing itself moved as a rigid body with flapping and pitching motion. The uncoupled bending and torsion frequencies and mode shapes, given in table II, were calculated by using beam theory for a rigid body on a flexible weightless shaft. These calculated mode shapes and frequencies compared well with measured values. The first measured natural mode was essentially uncoupled, while the second uncoupled mode was obtained experimentally by restraining the model at the elastic axis on the wing.

After the tests each model was cut into strips parallel to the airstream. The number of strips varied from nine for the 60° models to five for the 80° models. The spanwise variation of the mass was obtained from the weight of the individual strips. The mass moment of inertia was found by swinging the strips in a calibrated torsion pendulum. Table I(b) presents the distribution of mass, static unbalance, and inertia for each of the models. All the distributions in table I(b) have been corrected for the amount of material lost due to the saw cuts.

FLUTTER EXPERIMENTS

Apparatus

The tests were performed in the 24-inch-diameter leg of the Langley Mach 15 hypersonic aeroelasticity tunnel, which uses helium as a test medium. A description of this facility and its operating characteristics can be found in reference 3.

The models were mounted on a reflection plane which was supported 6.8 inches from the tunnel wall as shown in figure 1. The reflection-plane support structure was designed to insure that the model was out of the tunnel wall boundary layer. A clamping device was provided at the junction of the model shaft and reflection plane in the support structure. (See fig. 5.) This clamping device was used to restrain the model during the tunnel starting transient and also to avoid destruction of the model when flutter occurred. Thus, the same model could be used for more than one test.

Procedure

Models were mounted in the test section at zero angle of attack. After installation and just prior to each test run, the measurements for the first two natural frequencies of the models were checked. The tunnel was then evacuated to a pressure of 1/4 inch of mercury absolute. The model was restrained, and a control valve upstream of the test section was opened, and flow was established at dynamic pressure of about 100 psf. At this time the model was released and, with the Mach number remaining constant, the dynamic pressure was increased until flutter was encountered or the maximum tunnel operating conditions were reached. At that point the model was again restrained and the tunnel flow stopped.

Throughout the tests stagnation temperature and pressure were recorded on an oscillograph together with signals from resistance-type strain gages mounted on the model shaft (see fig. 2), so that tunnel conditions could be correlated with model behavior. Other pertinent tunnel data were obtained from helium flow tables. The strain-gage response was used to indicate the occurrence of flutter and to evaluate the flutter frequency. High-speed motion pictures of the flutter of most of the models were obtained.

FLUTTER CALCULATIONS

Two-degree-of-freedom flutter calculations were made for the models by using the first two uncoupled modes, since reference 1 showed that for models of this type flutter characteristics obtained by using uncoupled modes gave better agreement with experimental results than those obtained by using coupled modes. The aerodynamic parameters were obtained from second-order piston theory or from modified Newtonian theory. In both theories the local surface pressure generated by the wing motion is completely defined by the Mach number, the ratio of specific heats, and, for small flow angles, the component of the free-stream velocity normal to the wing surface. This component of velocity is given by

$$\frac{w}{V} = \mp\frac{dz}{dx} \pm \alpha_0 \pm \left[\frac{\dot{h}(t)}{V} + \alpha(t) + \frac{(x - x_0)}{V}\dot{\alpha}(t)\right] \tag{1}$$

where the first two terms correspond to the steady-state component of the downwash. Here the ~~negative~~ lower sign refers to the upper surface.

For piston theory (ref. 4) the pressure coefficient in terms of the downwash is given by

$$C_p = 2\left[\frac{1}{M}\left(\frac{w}{V}\right) + \frac{\gamma + 1}{4}\left(\frac{w}{V}\right)^2\right] \tag{2}$$

neglecting third and higher order terms. Valid application of this expression requires that the downwash velocity at the wing surface be less than the speed of sound. This requirement, besides being a limit on airfoil thickness, amplitude, and frequency of motion, also implies that piston theory will not be applicable near the leading edge of blunt-nosed airfoils where the surface slopes are large. For the piston-theory calculations of this study, the wing leading edge was assumed to be sharp with a wedge inscribed in the semiconical leading edge.

A hypersonic theory which does not have the leading-edge-bluntness limitation is Newtonian theory for which the pressure coefficient is $C_p = 2 \sin^2\phi$. Applications of Newtonian steady-flow theory in this form do not correlate too closely with experimental results for the stagnation point (ref. 5). However, a pressure coefficient of this type based on the stagnation pressure obtained from normal-shock relations gives better agreement. This modified Newtonian pressure coefficient which includes an unsteady component is given by

$$C_p = C_{p,stag} \sin^2(\phi \pm \theta) \tag{3}$$

where

$$\phi = \pm\alpha_0 + \tan^{-1}\frac{1}{dx/dz} \tag{4}$$

and, where

$$\theta = \left[\frac{\dot{h}(t)}{V} + \alpha(t) + \frac{(x - x_0)}{V}\dot{\alpha}(t)\right] \tag{5}$$

for small values of θ. Any point in the aerodynamic shadow, hidden from the free stream by a portion of the airfoil, is assumed to be in a region of zero pressure.

Expressions for the lift and pitching moment of the oscillating wing were obtained from equations (2) and (3). The resulting aerodynamic coefficients obtained from piston theory are tabulated in reference 6 for a variety of airfoils including those used in this investigation. Expressions for the corresponding aerodynamic coefficients based on modified Newtonian theory are given in the appendix of this report. All flutter speeds were computed by using these aerodynamic derivatives incorporated into the strip method of reference 7.

RESULTS AND DISCUSSION

Experimental Results

The results of the wind-tunnel test are given in table II, which lists the flow conditions at flutter as well as the flutter-frequency ratio ω_f/ω_2 and flutter-speed index, $V/b_r\omega_2\sqrt{\mu}$, for each run where flutter occurred. Four of the fifteen models tested did not encounter flutter; the data given for those models are the maximum tunnel conditions reached during the test. The experimental results from table II are presented in figures 6 and 7 as the variation of the flutter-speed index and the flutter-frequency ratio with leading-edge-sweep angle, respectively. In figure 8, the data of reference 1 are combined with the present data and are given as the variation of flutter-speed index with Mach number for the wedge and double-wedge airfoils.

Figure 6 shows three curves - one for each of the airfoil shapes. These data reveal that for each leading-edge-sweep angle the slab airfoil is the most stable while the double-wedge airfoil is the least stable. All three series of airfoils indicate that increasing the leading-edge-sweep angle from 60° to about 65° or 70° is destabilizing, while further increases in sweep are stabilizing. However, these trends may be influenced by the layer of disturbed flow along the reflection-plane surface which will be discussed later. It can be seen in figure 7 that the flutter frequency always falls between the first two natural

frequencies. The motion pictures taken during the test indicated that the models had a flapping-pitching type of flutter motion.

For wedge and double-wedge airfoils, figure 8 shows the trend of flutter-speed index when the Mach number is increased from 7.0 to 15.4. The airfoils with leading-edge-sweep angles up to 65° or 70° exhibit a slight destabilizing trend with increase in Mach number. For the higher swept airfoils the Mach number trend reverses with the models becoming consistently more stable with increases in leading-edge sweep.

The reflection-plane survey in figure 9 shows a disturbed flow region (shock layer) building up along the reflection-plane surface. (Fig. 9 was reproduced from ref. 3 since the same reflection plane was used in ref. 3 and in the present investigation in the same facility.) This layer is about 1.5 inches thick at the trailing edge of the models of this investigation. This layer covers between 75- and 100-percent semispan of the highly swept models at the trailing edge and about 20 percent at the trailing edge of the 60° model.

The presence of this disturbed layer undoubtedly influences the flutter characteristics of all the models and probably causes very large effects for the most highly swept surfaces. The magnitude of these effects would be difficult to evaluate because of the inherent difficulty in obtaining thin boundary layers at hypersonic speeds. A free-flying vehicle operating at hypersonic speeds would probably also have a relatively thick disturbed layer lying along its body and it is speculated that a similar influence on the flutter characteristics of a control surface attached to the body might occur in flight.

Comparisons With Theoretical Results

The effects of varying mass ratio μ on the flutter-speed index were calculated by using Newtonian theory for the range of experimental mass ratios encountered during the investigation. Over this range, the flutter-speed index was essentially independent of mass ratio.

The results of the flutter calculations are listed in table III and presented in figures 10 and 11. Figure 10 presents the ratio of experimental flutter speed to corresponding values calculated by piston theory and by Newtonian theory as a function of leading-edge sweep. The Newtonian theory always predicted the flutter speed more closely, while the piston theory was consistently conservative; it was most conservative in predicting the flutter speed for the slab series of airfoils. Such a difference is not surprising since the slab airfoils have the largest leading-edge radii, and piston theory does not take into account leading-edge bluntness. For the piston-theory calculations the leading edge was arbitrarily assumed to be sharp (as previously described). The calculated results might be slightly different if the leading edge had been treated in a different manner. Both theories roughly predict the flutter-speed trend with leading-edge sweep for angles up to 70° for the slab and double-wedge airfoils and to 75° for the wedge airfoils. However, neither theory predicted the increase in experimental flutter speed at higher sweep angles, probably because the theory does not account for flow conditions within the shock layer which covers most of the 80° surfaces. Another factor affecting the calculated

results is the approximation involved in applying two-dimensional strip theory to such a low-aspect-ratio delta planform. Two-dimensional strip theory was used in order to coincide with the procedure in reference 1, so that the results would be directly comparable. The panel aspect ratio of the 60°, 75°, and 80° models is 1.15, 0.54, and 0.35, respectively.

The ratio of experimental to theoretical flutter frequency is presented in figure 11 as a function of leading-edge-sweep angle for the three series of airfoils. Both theories gave fair prediction of the flutter frequency for the wedge and double-wedge airfoils. The correlation was poorer for the slab airfoils.

SUMMARY OF RESULTS

A wind-tunnel investigation has been conducted in helium flow at a Mach number of 15.4 to determine some effects of leading-edge-sweep angles and profile shape on the flutter characteristics of some delta planform all-movable control surfaces. The profiles tested were blunted wedges, double wedges, and slabs with leading-edge-sweep angles from 60° to 80°. The test indicated that increasing the leading-edge-sweep angle from 60° to about 65° or 70° is destabilizing, while further increases in sweep are stabilizing. However, these trends may be influenced by the layer of disturbed flow along the reflection-plane surface, particularly for the more highly swept models. At each sweep angle, the results show that the slab airfoils are the most stable while the double-wedge airfoils are the least stable. Combining the results of this investigation with the results of NASA TM X-325 at a Mach number of 7.0 shows a slight destabilizing trend with increase in Mach number for models having leading-edge-sweep angles up to 65° or 70°. For the more highly swept airfoils the trend becomes stabilizing.

Flutter calculations made by piston theory and modified Newtonian theory aerodynamics indicate that in all cases the Newtonian theory more closely predicted the experimental flutter speeds, particularly for the airfoils with large leading-edge radii.

Langley Research Center,
National Aeronautics and Space Administration,
Langley Station, Hampton, Va., March 7, 1964.

APPENDIX

AERODYNAMIC COEFFICIENTS BASED ON NEWTONIAN THEORY

On a two-dimensional airfoil with a blunt leading edge the normal-pressure

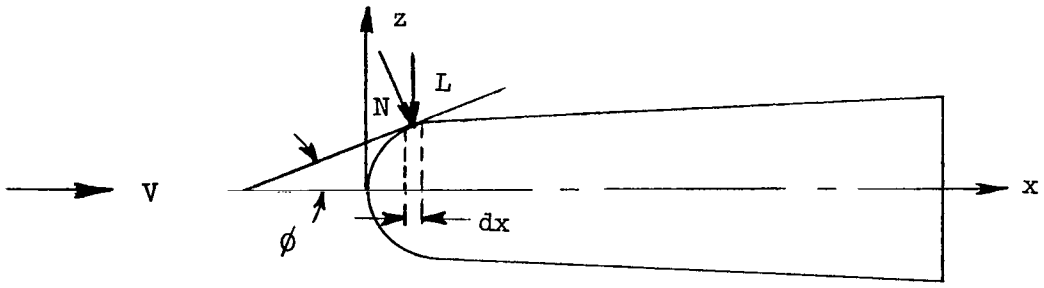

Body-axis system

coefficient as given by modified Newtonian theory according to reference 8 is

$$C_p = C_{p,stag} \sin^2\phi \tag{A1}$$

If the airfoil rotates through a small angle θ the coefficient becomes

$$C_p = C_{p,stag} \sin^2(\phi \pm \theta)$$

(see eqs. (4) and (5)) or

$$C_p = C_{p,stag}\left(\sin^2\phi \cos^2\theta \pm 2 \sin\phi \cos\theta \sin\theta \cos\phi + \cos^2\phi \sin^2\theta\right)$$

for $0 \leqq \phi \leqq \pi/2$ and

$$C_p = -\frac{2p_\infty}{\rho V^2}$$

for $\phi < 0$ where the latter form applies in the aerodynamic shadow. The negative sign corresponds to the upper surface. The pressure-coefficient difference between the upper and lower surface can be written as

$$C_{p,l} - C_{p,u} = C_{p,stag}(4 \cos \phi \sin \theta \sin \phi \cos \theta) \tag{A2}$$

for a symmetrical airfoil with no surface in the aerodynamic shadow. Making a rectangular-coordinate substitution and assuming zero initial angle of attack,

$$\cos \phi = \frac{dx/dz}{\sqrt{1 + \left(\frac{dx}{dz}\right)^2}} \tag{A3a}$$

and

$$\sin \phi = \frac{1}{\sqrt{1 + \left(\frac{dx}{dz}\right)^2}} \tag{A3b}$$

and recalling that θ is assumed to be small, gives the pressure-coefficient difference reduced to

$$C_{p,l} - C_{p,u} = C_{p,stag}\, 4\left[\frac{dx/dz}{1 + \left(\frac{dx}{dz}\right)^2}\right]\theta \tag{A4a}$$

If θ varies with time and consists of combined pitching and plunging then from equation (5)

$$C_{p,l} - C_{p,u} = C_{p,stag}\, 4\left[\frac{dx/dz}{1 + \left(\frac{dx}{dz}\right)^2}\right]\left\{\alpha(t) \pm \left[\dot{h}(t) + \left(x - x_0\right)\dot{\alpha}(t)\right]\frac{1}{V}\right\} \tag{A4b}$$

where $\alpha(t)$ is the angular perturbation of the wing about zero angle of attack and $h(t)$ is the vertical displacement of the elastic axis (both as a function of time). For simple harmonic motion the lift equation can be written directly as

$$-L = \int_{x_{LE}}^{x_{TE}} \Delta p\,dx = \int_{x_{LE}}^{x_{TE}} \frac{\rho V^2}{2}\left(C_{p,l} - C_{p,u}\right)dx$$

$$= 2\rho V^2 C_{p,stag}\left\{\int_{x_{LE}}^{x_{TE}} Z_N\left[\frac{i\omega}{V}\,h(t) + \alpha(t) + \frac{\left(x - x_0\right)i\omega}{V}\,\alpha(t)\right]dx\right\} \tag{A5}$$

Similarly, the moment due to pitching and plunging can be written as

$$-M_\alpha = \int_{x_{LE}}^{x_{TE}} \left(x - \bar{x}_0\right)\Delta p\,dx = 2\rho V^2 C_{p,stag} \int_{x_{LE}}^{x_{TE}} Z_N\left(x - x_0\right)\left[\frac{i\omega h(t)}{V} + \alpha(t)\right.$$

$$\left. + \left(x - x_0\right)\frac{i\omega}{V}\,\alpha(t)\right]dx \tag{A6}$$

where Z_N is the function $\dfrac{dx/dz}{1 + \left(\dfrac{dx}{dz}\right)^2}$, defined by the airfoil shape. For high-speed-computer calculations, it is convenient to use the form of Garrick and Rubinow, reference 9 in which

$$L = -4\rho V^2 b_r k_r{}^2\left[\left(L_1 + iL_2\right)\frac{h(t)}{b_r} + \left(L_3 + iL_4\right)\alpha(t)\right] \tag{A7}$$

and

$$M_\alpha = -4\rho V^2 b_r{}^2 k_r{}^2\left[\left(M_1 + iM_2\right)\frac{h(t)}{b_r} + \left(M_3 + iM_4\right)\alpha(t)\right] \tag{A8}$$

where the nondimensional aerodynamic coefficients given by Newtonian theory are

$$L_1 = 0$$

$$L_2 = \frac{C_{p,stag}}{2b_r k_r}\int_{x_{LE}}^{x_{TE}} Z_N dx$$

$$L_3 = \frac{C_{p,stag}}{2b_r k_r^2} \int_{x_{LE}}^{x_{TE}} Z_N dx = \frac{1}{k_r} L_2$$

$$L_4 = \frac{C_{p,stag}}{2b_r^2 k_r} \int_{x_{LE}}^{x_{TE}} Z_N \left(x - x_0\right) dx$$

$$M_1 = 0$$

$$M_2 = \frac{C_{p,stag}}{2b_r^2 k_r} \int_{x_{LE}}^{x_{TE}} Z_N \left(x - x_0\right) dx = L_4$$

$$M_3 = \frac{C_{p,stag}}{2b_r^2 k_r^2} \int_{x_{LE}}^{x_{TE}} Z_N \left(x - x_0\right) dx = \frac{1}{k_r} M_2$$

$$M_4 = \frac{C_{p,stag}}{2b_r^3 k_r} \int_{x_{LE}}^{x_{TE}} Z_N \left(x - x_0\right)^2 dx$$

For a hemicylindrical leading edge where $Z_N = \frac{(r - x)\left(2rx - x^2\right)^{1/2}}{r^2}$ the aerodynamic coefficients reduce to

$$L_1 = 0$$

$$L_2 = \frac{C_{p,stag}}{3k_r} \left(\frac{b}{b_r}\right) \overline{r}$$

$$L_3 = \frac{1}{k_r} L_2$$

$$L_4 = \frac{2C_{p,stag}}{3k_r} \left(\frac{b}{b_r}\right)^2 \left(\frac{16\overline{r}^2 - 3\pi\overline{r}^2}{16} - \overline{rx}_0\right)$$

and

$$M_1 = 0$$

$$M_2 = L_4$$

$$M_3 = \frac{1}{k_r} L_4$$

$$M_4 = \frac{4C_{p,stag}}{k_r}\left(\frac{b}{b_r}\right)^3\left[\overline{r}^3\left(\frac{7}{15} - \frac{\pi}{8}\right) + \overline{r}^2\overline{x}_0\left(\frac{\pi}{8} - \frac{2}{3}\right) + \frac{\overline{rx}_0^2}{3}\right]$$

REFERENCES

1. Miller, Robert W., and Hannah, Margery E.: Flutter Investigation of 60° to 80° Delta-Planform Surfaces at a Mach Number of 7.0. NASA TM X-325, 1960.

2. Herr, Robert W.: Preliminary Experimental Investigation of Flutter Characteristics of M and W Wings. NACA RM L51E31, 1951.

3. Goetz, Robert C.: Effects of Leading-Edge Bluntness on Flutter Characteristics of Some Square-Planform Double-Wedge Airfoils at a Mach Number of 15.4. NASA TN D-1487, 1962.

4. Morgan, Homer G., Runyan, Harry L., and Huckel, Vera: Theoretical Considerations of Flutter at High Mach Numbers. Jour. Aero. Sci., vol. 25, no. 6, June 1958, pp. 371-381.

5. Bertram, Mitchel H., and Henderson, Arthur, Jr.: Recent Hypersonic Studies of Wings and Bodies. ARS Jour., vol. 31, no. 8, Aug. 1961, pp. 1129-1139.

6. Chawla, Jagannath P.: Aeroelastic Instability at High Mach Number. Jour. Aero. Sci., vol. 25, no. 4, April 1958, pp. 246-258.

7. Barmby, J. G., Cunningham, H. J., and Garrick, I. E.: Study of Effects of Sweep on the Flutter of Cantilever Wings. NACA Rep. 1014, 1951. (Supersedes NACA TN 2121.)

8. Lees, Lester: Hypersonic Flow. Fifth International Aeronautical Conference (Los Angeles, Calif., June 20-23, 1955), Inst. Aero. Sci., Inc., 1955, pp. 241-276.

9. Garrick, I. E., and Rubinow, S. I.: Flutter and Oscillating Air-Force Calculations for an Airfoil in Two-Dimensional Supersonic Flow. NACA Rep. 846, 1946. (Supersedes NACA TN 1158.)

TABLE I.- MEASURED MODEL PROPERTIES

(a) Overall properties

$\left[\bar{x}_{0_{\text{root}}} = 0.65\right]$

Model (a)	Mass, m, slugs	$\bar{x}_{cg}$, percent root chord	$\bar{y}_{cg}$, percent semispan	I_α, slugs-ft^2	r_α^2	Wing root semichord, b_r, ft	Wing semispan, s, ft	Shaft length, ℓ, in.	Shaft thickness, d, in.	Natural frequencies				
										f_1, cps	f_2, cps	f_3, cps	f_4, cps	f_1/f_2
60-W-1	0.01404	70.9	19.7	4.485×10^{-4}	0.184	0.417	0.4811	4.30	0.0625	8.45	19.6	80.6	352.0	0.43
65-W-1	.01248	71.0	19.5	3.789	.175		.3886	4.31	.0625	9.60	20.6	101.9	502.6	.47
70-W-1	.01092	71.1	21.3	3.169	.167		.3033	4.30	.0625	9.56	20.7	132.8	594.0	.46
75-W-1	.00912	71.2	19.8	2.642	.167		.2233	4.85	.0625	10.90	23.6	161.7	552.5	.46
80-W-1	.00672	71.4	17.5	1.842	.158		.1469	5.18	.0625	12.30	26.4	199.2	548.2	.47
60-DW-2	.01632	69.2	17.7	4.823	.170		.4811	3.35	.0625	9.76	22.5	95.0	327.8	.43
65-DW-2	.01572	69.3	18.0	3.975	.145		.3886	3.50	.0625	9.71	21.4	107.3		.45
70-DW-2	.01536	70.9	21.3	4.533	.170		.3033	4.25	.0625	8.77	20.5	110.8	635.0	.43
75-DW-2	.01176	68.5	18.3	2.922	.143		.2233	4.66	.0625	9.72	21.2	151.5	589.0	.46
80-DW-2	.00852	68.6	21.5	2.003	.135		.1469	4.92	.0625	11.46	24.25	198.5	570.0	.47
60-S-1	.02048	68.5	17.0	7.011	.197		.4811	5.50	.0625	5.66	12.65	55.6		.45
65-S-1	.01837	69.0	16.9	6.392	.200		.3886	5.80	.0625	5.79	12.9	69.6		.45
70-S-1	.01583	68.4	17.3	5.254	.191		.3033	6.00	.0625	6.09	13.35	88.3	352.5	.46
75-S-1	.01343	68.6	16.8	4.399	.189		.2233		.0625	6.67	14.5	114.4	359.0	.46
80-S-1	.00961	68.8	16.0	3.105	.186		.1469	6.25	.0625	8.06	16.9	146.9	397.0	.48
75-W-2	.00912	71.2	19.8	2.642	.167		.2233	5.00	.050	7.63	16.66	138.0		.46
75-W-3	.00912	71.2	19.8	2.642	.167		.2233	5.00	.041	5.54	12.20	88.9		.45
80-W-2	.00672	71.4	17.5	1.842	.158		.1469	5.25	.040	6.67	14.0	115.0		.46
80-W-3	.00672	71.4	17.5	1.842	.158		.1469	5.50	.031	3.87	8.75	73.4		.44
75-DW-3	.01176	68.5	18.3	2.922	.143		.2233	5.00	.050	6.21	14.45	101.0		.43
80-DW-3	.00852	68.6	21.5	2.003	.135		.1469	6.00	.041	5.53	11.66	93.8		.47
70-S-2	.01583	68.4	17.3	5.254	.191		.3033	5.95	.050	4.27	9.46	65.2		.45
75-S-2	.01343	68.6	16.8	4.399	.189		.2233	6.00	.0415	3.86	7.94	69.3		.49
80-S-2	.00961	68.8	16.0	3.105	.186	↓	.1469	6.00	.032	3.20	6.48	65.4		.49

[a]In the model designations, the first two integers indicate the leading-edge-sweep angle Λ in degrees; the letters indicate the profile shape (W-wedge; DW-double wedge; S-slab); the last integer indicates the stiffness level of the model $\left[3 < 2 < 1\right]$.

TABLE I.- MEASURED MODEL PROPERTIES - Continued

(b) Distributed properties

Model 60-W-1

Strip	δ, in.	Weight, lb	S_α, lb-in.	I_{ea}, lb-in-sec^2
1 (root)	0.75	0.2222	0.0184	33.81×10^{-4}
2	↓	.1180	.1097	14.25
3		.0400	.0147	3.21
4		.0315	.0296	2.20
5		.0213	.0345	2.07
6		.0126	.0278	1.82
7 (tip)		.0041	.0116	.91
Totals		0.4497		58.27×10^{-4}

Model 65-W-1

Strip	δ, in.	Weight, lb	S_α, lb-in.	I_{ea}, lb-in-sec^2
1 (root)	0.45	0.1441	-0.0101	18.95×10^{-4}
2	↓	.1075	.0489	10.64
3		.0679	.0714	7.28
4		.0275	.0202	2.07
5		.0192	.0170	1.39
6		.0150	.0198	1.26
7		.0108	.0195	1.17
8		.0066	.0150	1.05
9 (tip)		.0025	.0069	.55
Totals		0.4011		44.36×10^{-4}

Model 70-W-1

Strip	δ, in.	Weight, lb	S_α, lb-in.	I_{ea}, lb-in-sec^2
1 (root)	0.56	0.1626	0	21.29×10^{-4}
2	↓	.1065	.0817	9.19
3		.0476	.0639	5.36
4		.0194	.0252	1.62
5		.0109	.0221	1.43
6 (tip)		.0035	.0095	.73
Totals		0.3505		39.62×10^{-4}

Model 75-W-1

Strip	δ, in.	Weight, lb	S_α, lb-in.	I_{ea}, lb-in-sec^2
1 (root)	0.50	0.1421	0.0125	17.50×10^{-4}
2	↓	.0906	.0680	7.97
3		.0444	.0666	4.67
4		.0127	.0226	1.44
5 (tip)		.0035	.0088	.64
Totals		0.2933		32.22×10^{-4}

Model 80-W-1,2,3

Strip	δ, in.	Weight, lb	S_α, lb-in.	I_{ea}, lb-in-sec^2
1 (root)	0.30	0.0938	0	11.58×10^{-4}
2	↓	.0644	.0336	5.43
3		.0357	.0414	3.07
4		.0173	.0303	1.99
5 (tip)		.0048	.0113	.83
Totals		0.2160		22.90×10^{-4}

Model 65-DW-1

Strip	δ, in.	Weight, lb	S_α, lb-in.	I_{ea}, lb-in-sec^2
1 (root)	0.45	0.1628	-0.1148	20.23×10^{-4}
2	↓	.1143	.0101	8.39
3		.0643	.0488	5.08
4		.0496	.0524	3.94
5		.0461	.0625	3.72
6		.0304	.0461	2.60
7		.0239	.0426	2.43
8		.0135	.0280	1.83
9 (tip)		.0022	.0059	.48
Totals		0.5071		48.70×10^{-4}

Model 70-DW-1

Strip	δ, in.	Weight, lb	S_α, lb-in.	I_{ea}, lb-in-sec^2
1 (root)	0.55	0.1874	-0.0987	23.25×10^{-4}
2	↓	.1276	.0614	9.62
3		.0727	.0964	6.66
4		.0603	.1030	5.98
5		.0402	.0803	4.83
6 (tip)		.0058	.0148	1.08
Totals		0.4940		51.42×10^{-4}

Model 75-DW-1

Strip	δ, in.	Weight, lb	S_α, lb-in.	I_{ea}, lb-in-sec^2
1 (root)	0.50	0.1696	-0.0953	20.39×10^{-4}
2	↓	.1060	.0473	6.95
3		.0616	.0878	5.22
4		.0336	.0648	3.97
5 (tip)		.0062	.0154	1.12
Totals		0.3770		37.65×10^{-4}

Model 80-DW-1

Strip	δ, in.	Weight, lb	S_α, lb-in.	I_{ea}, lb-in-sec^2
1 (root)	0.30	0.1129	-0.0586	13.85×10^{-4}
2	↓	.0798	.0234	5.54
3		.0501	.0553	3.47
4		.0249	.0426	2.55
5 (tip)		.0057	.0130	.91
Totals		0.2734		26.32×10^{-4}

TABLE I.- MEASURED MODEL PROPERTIES - Concluded

(b) Distributed properties - Concluded

Model 60-S-1

Strip	δ, in.	Weight, lb	S_α, lb-in.	Iea, lb-in-sec^2
1 (root)	0.75	0.3668	-0.0714	48.40 × 10^{-4}
2		.1593	.1388	18.24
3		.0527	.0122	4.74
4		.0381	.0335	2.81
5		.0236	.0370	2.31
6		.0142	.0315	2.18
7 (tip)	↓	.0043	.0121	.95
Totals		0.6590		79.63 × 10^{-4}

Model 65-S-1

Strip	δ, in.	Weight, lb	S_α, lb-in.	Iea, lb-in-sec^2
1 (root)	0.45	0.2421	-0.1074	42.21 × 10^{-4}
2		.1568	.0956	18.01
3		.1005	.1040	11.38
4		.0327	.0217	2.94
5		.0235	.0215	1.66
6		.0175	.0249	1.50
7		.0097	.0189	1.27
8		.0062	.0151	1.16
9 (tip)	↓	.0017	.0051	.42
Totals		0.5907		80.55 × 10^{-4}

Model 70-S-1,2

Strip	δ, in.	Weight, lb	S_α, lb-in.	Iea, lb-in-sec^2
1 (root)	0.56	0.2834	-0.0703	45.57 × 10^{-4}
2		.1346	.0902	12.65
3		.0490	.0662	5.55
4		.0217	.0279	1.74
5		.0117	.0239	1.66
6 (tip)	↓	.0037	.0101	.78
Totals		0.5041		67.95 × 10^{-4}

Model 75-S-1,2

Strip	δ, in.	Weight, lb	S_α, lb-in.	Iea, lb-in-sec^2
1 (root)	0.50	0.2418	-0.0659	38.17 × 10^{-4}
2		.1240	.0957	10.76
3		.0494	.0736	5.11
4		.0135	.0248	1.58
5 (tip)	↓	.0035	.0092	.68
Totals		0.4322		56.30 × 10^{-4}

Model 80-S-1

Strip	δ, in.	Weight, lb	S_α, lb-in.	Iea, lb-in-sec^2
1 (root)	0.30	0.1602	-0.0519	24.41 × 10^{-4}
2		.0879	.0555	9.78
3		.0392	.0468	2.92
4		.0172	.0312	2.02
5 (tip)	↓	.0043	.0107	.80
Totals		0.3088		39.93 × 10^{-4}

TABLE II.- EXPERIMENTAL RESULTS

Model	Run	Model behavior (a)	Mach number, M	Dynamic pressure, $\rho V^2/2$, lb/sq ft	Density, ρ, slugs/cu ft	Speed of sound, a, ft/sec	Mass ratio, μ	Speed, V, ft/sec	Frequency, ω_2, radians/sec	$V/b_r\omega_2\sqrt{\mu}$	ω_f, radians/sec	ω_f/ω_2	Reynolds number, R
60-W-1	2	f	15.3	331.9	1.626×10^{-5}	417.6	9,859.6	6,389.3	123.2	1.253	79.17	0.643	1.660×10^6
65-W-1	3	f	15.4	361.4	1.814	409.9	9,734.8	6,312.5	129.4	1.186	85.45	.660	1.718
70-W-1	4	f	15.4	467.0	2.659	384.8	7,443.8	5,925.9	130.1	1.266	88.59	.681	2.590
75-W-1	5	nf	15.4	579.5	3.277	386.2	6,852.0	5,947.5	148.3	1.162			3.171
80-W-1	1	nf	15.4	562.9	3.274	380.8	7,671.2	5,864.3	165.9	.968			3.170
75-W-2	9	nf	15.4	553.5	3.231	380.1	6,951.2	5,853.5	104.7	1.608			3.121
75-W-3	22	f	15.3	290.9	1.612	392.6	13,875.0	6,006.8	76.7	1.594	44.86	.585	1.154
80-W-2	10	nf	15.4	571.5	3.289	382.8	7,636.4	5,895.1	88.0	1.838			3.186
80-W-3	21	nf	15.4	595.3	3.372	385.9	7,441.9	5,942.9	55.0	3.004			3.262
70-W-1	25	f	15.4	465.0	2.713	380.2	7,295.6	5,855.1	130.1	1.264	87.90	.676	2.589
60-DW-2	11	f	15.4	415.7	2.303×10^{-5}	390.2	8,091.2	6,009.1	141.4	1.133	92.55	.655	2.226×10^6
65-DW-2	13	f		368.4	1.926	401.6	11,550.3	6,184.6	134.5	1.026	83.69	.622	1.837
70-DW-2	8	f		359.0	1.856	403.9	15,000.0	6,220.1	128.8	.946	75.40	.585	1.768
75-DW-2	14	nf		571.5	3.221	386.8	8,990.8	5,956.7	133.2	1.131			3.116
80-DW-2	15	nf		567.6	3.325	379.4	9,573.0	5,842.8	152.4	.940			3.214
75-DW-3	23	f		451.2	2.458	393.5	11,783.5	6,059.9	90.8	1.474	59.88	.659	2.369
80-DW-3	24	nf		576.0	3.315	382.8	9,605.4	5,895.1	73.3	1.968			3.210
70-DW-2	26	f	↓	350.5	1.843	400.5	15,105.8	6,167.7	128.8	.934	69.12	.537	1.770
60-S-1	16	f	15.4	406.2	2.209×10^{-5}	393.8	10,584.0	6,064.5	79.5	1.778	62.83	.790	2.129×10^6
65-S-1	17	f	15.2	282.2	1.464	408.5	17,766.0	6,209.2	81.1	1.377	57.99	.715	1.484
70-S-1	18	nf	15.4	559.9	3.245	381.4	8,838.6	5,873.6	83.9	1.786			3.140
70-S-2	19	f	15.4	477.1	2.599	393.5	11,039.1	6,059.9	59.4	2.328	38.61	.650	2.505
75-S-2	20	nf	15.4	583.5	3.388	381.1	9,760.2	5,868.9	49.9	2.855			3.279
65-S-1	27	f	15.3	290.0	1.549	400.0	16,791.1	6,120.0	81.1	1.396	56.55	.697	1.490

[a] f - flutter.
nf - no flutter.

TABLE III.- THEORETICAL RESULTS

Model	Run	Experimental model behavior (a)	Piston theory				Newtonian theory				ω_h, radians/sec	ω_α, radians/sec	Uncoupled bending mode shape
			V_{th}, ft/sec	$\omega_{f,th}$, radians/sec	V_{ex}/V_{th}	$\omega_{f,ex}/\omega_{f,th}$	V_{th}, ft/sec	$\omega_{f,th}$, radians/sec	V_{ex}/V_{th}	$\omega_{f,ex}/\omega_{f,th}$			
60-W-1	2	f	4645	73.83	1.376	1.072	6863	82.56	0.931	0.959	57.10	121.7	$1.0 + 2.200x/l$
65-W-1	3	f	3632	79.67	1.738	1.073	5402	90.67	1.169	.942	64.34	132.7	$1.0 + 1.756x/l$
70-W-1	4	f	3854	88.09	1.538	1.006	5648	101.16	1.049	.876	70.09	145.3	$1.0 + 1.367x/l$
75-W-1	5		5541	71.69	1.073						71.83	149.7	$1.0 + 0.866x/l$
80-W-1	1	nf	3575	101.54	1.640		5393	112.91	1.087		83.07	174.4	$1.0 + 0.520x/l$
75-W-2	9	nf	3903	49.51	1.500		6857	56.36	.854		49.09	104.9	$1.0 + 0.842x/l$
75-W-3	22	f	4647	36.57	1.293	1.227	6318	43.05	.950	1.041	36.33	77.7	$1.0 + 0.842x/l$
80-W-2	10	nf	1800	50.83	3.275		2715	56.55	2.171		41.35	87.6	$1.0 + 0.515x/l$
80-W-3	21	nf	1207	32.99	4.924		1804	36.82	3.294		26.25	58.1	$1.0 + 0.490x/l$
70-W-1	25	f	3854	88.09	1.519	.998	5648	101.16	1.037	.869	70.09	145.3	$1.0 + 1.367x/l$
60-DW-2	11		----	------			----	------	-----	-----	78.10	129.6	$1.0 + 2.823x/l$
65-DW-2	13	f	3521	84.07	1.756	.995	4221	83.44	1.465	1.003	79.37	139.6	$1.0 + 2.152x/l$
70-DW-2	8	f	4361	66.67	1.426	1.131	5332	68.80	1.167	1.096	58.82	118.7	$1.0 + 1.390x/l$
75-DW-2	14	nf	3868	75.78	1.540		4774	80.11	1.248		67.38	141.4	$1.0 + 0.902x/l$
80-DW-2	15	nf	3887	87.59	1.503		4778	91.74	1.223		75.83	166.1	$1.0 + 0.556x/l$
75-DW-3	23	f	3117	51.77	1.944	1.157	3827	53.09	1.583	1.128	43.70	96.9	$1.0 + 0.839x/l$
80-DW-3	24	f	1972	38.27	2.989		2397	40.09	2.459		30.30	79.05	$1.0 + 0.453x/l$
70-DW-2	26	f	4361	66.67	1.414	1.037	5332	68.80	1.157	1.005	58.82	118.7	$1.0 + 1.390x/l$
60-S-1	16	f	3170	46.50	1.913	1.351	6661	42.98	.910	1.462	36.19	85.2	$1.0 + 1.686x/l$
65-S-1	17	f	3429	48.70	1.811	1.191	6901	44.30	.901	1.310	37.28	86.9	$1.0 + 1.273x/l$
70-S-1	18	nf	2945	52.59	1.994		6193	48.26	.948		39.87	94.3	$1.0 + 0.950x/l$
70-S-2	19	f	2340	37.51	2.590	1.029	4908	34.24	1.235	1.127	29.71	67.3	$1.0 + 0.961x/l$
75-S-2	20	nf	1613	30.16	3.638		3386	28.02	1.733		24.15	54.2	$1.0 + 0.692x/l$
65-S-1	27	f	3429	48.70	1.785	1.161	6901	44.30	.887	1.277	37.28	86.9	$1.0 + 1.273x/l$

[a] f - flutter.
nf - no flutter.

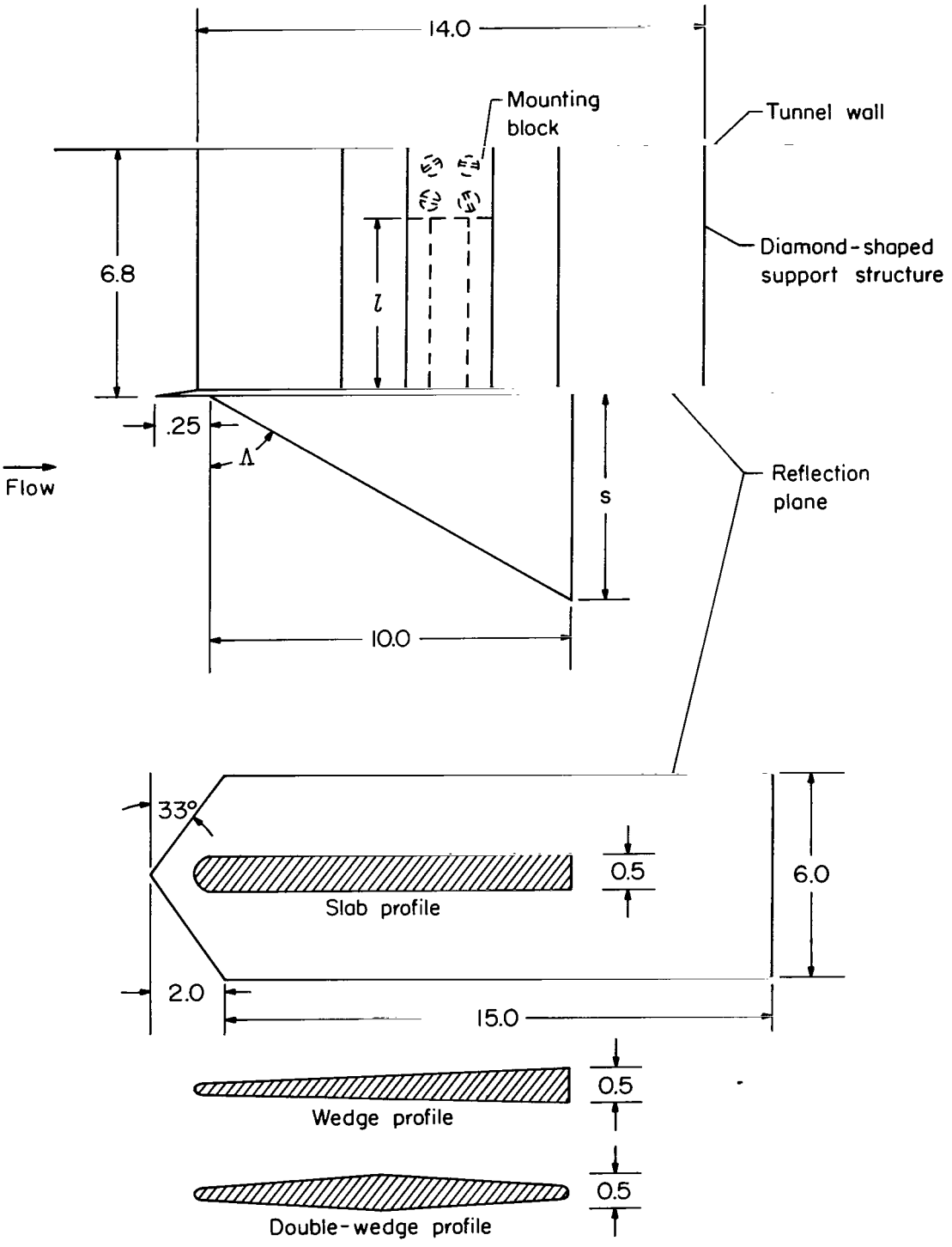

Figure 1.- Sketch of models and their support structure. All dimensions are in inches unless otherwise stated.

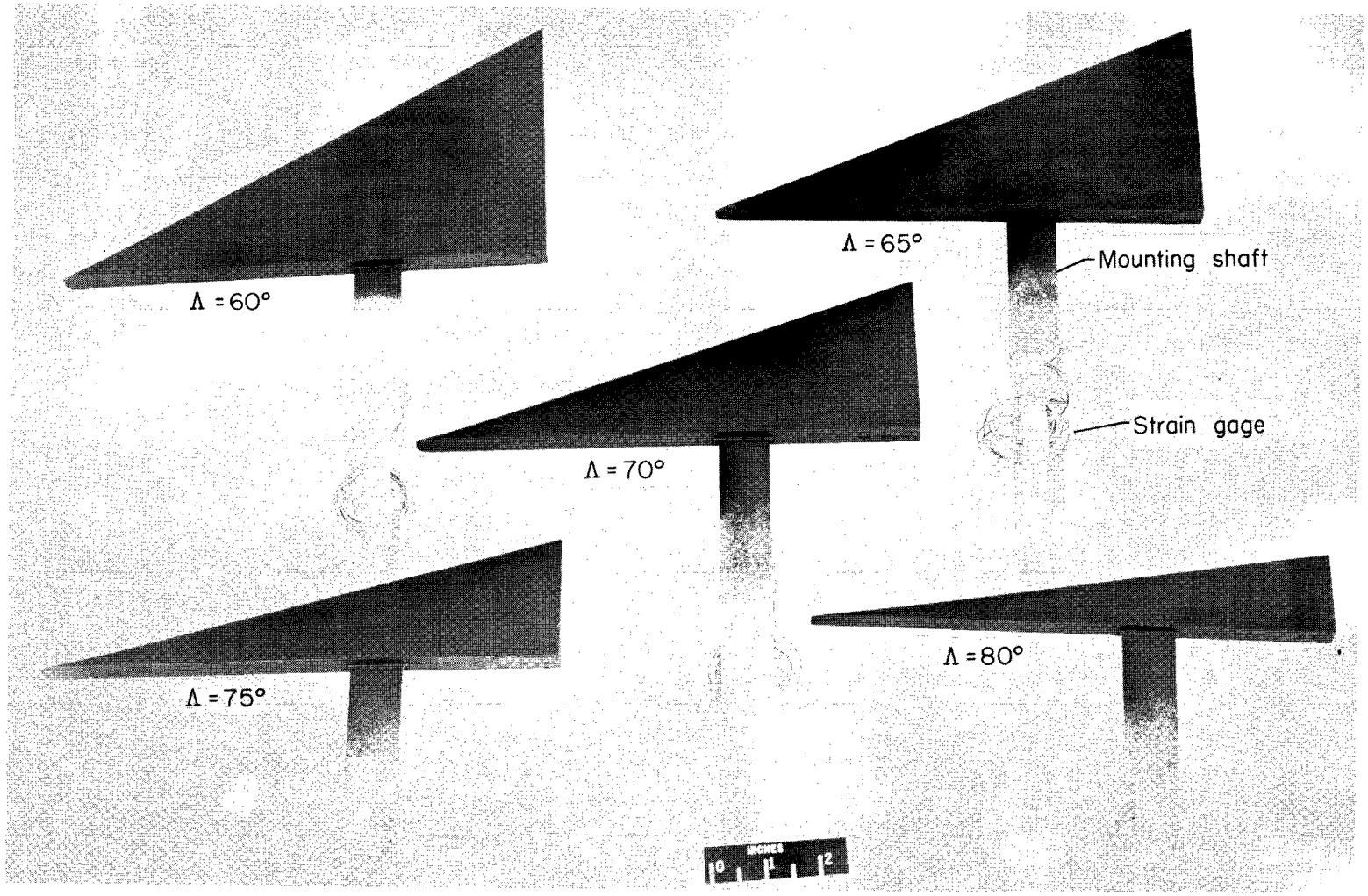

Figure 2.- Planforms.

L-61-7050.1

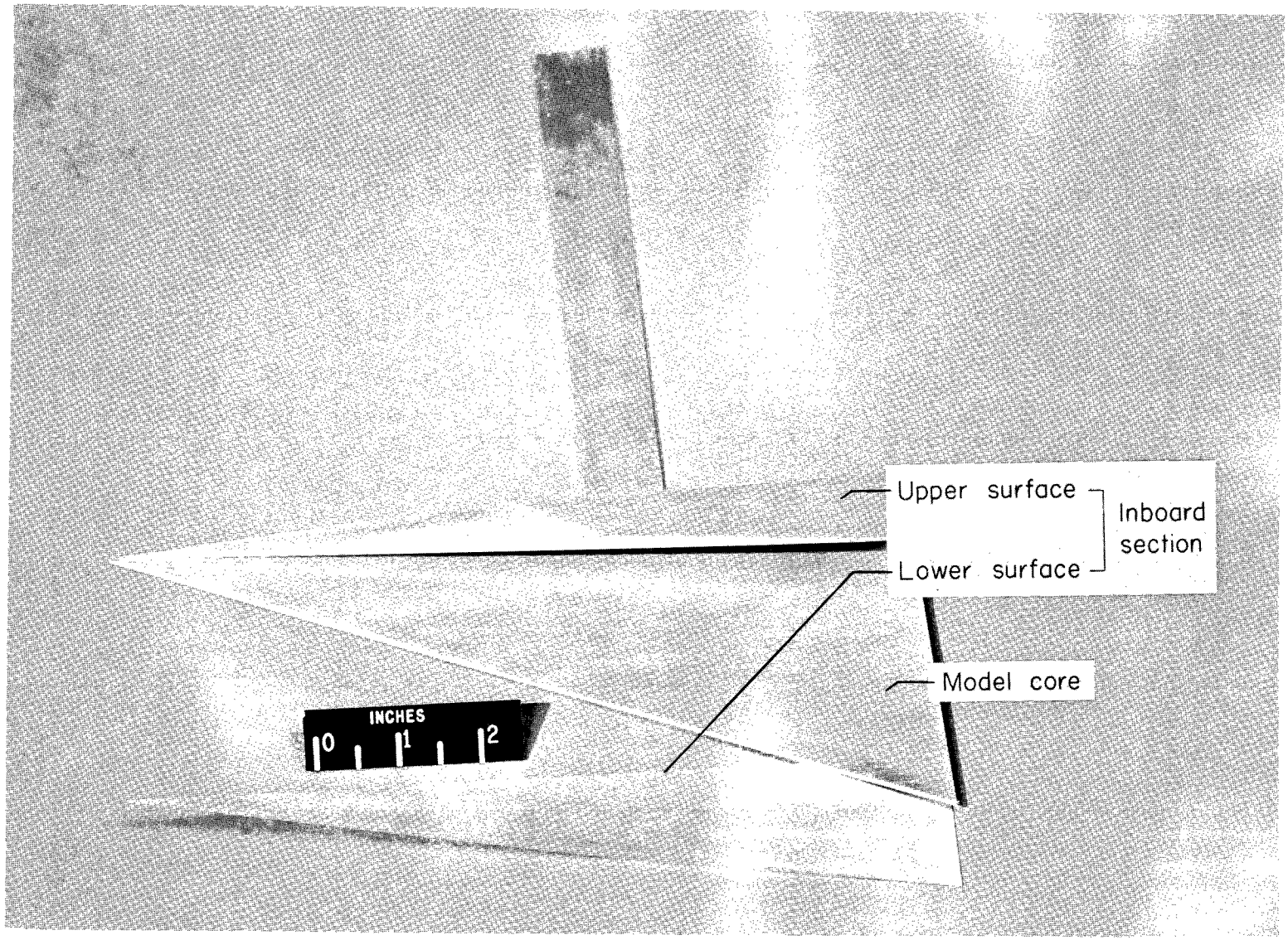

Figure 3.- Metal portion of typical model.

L-61-3646.1

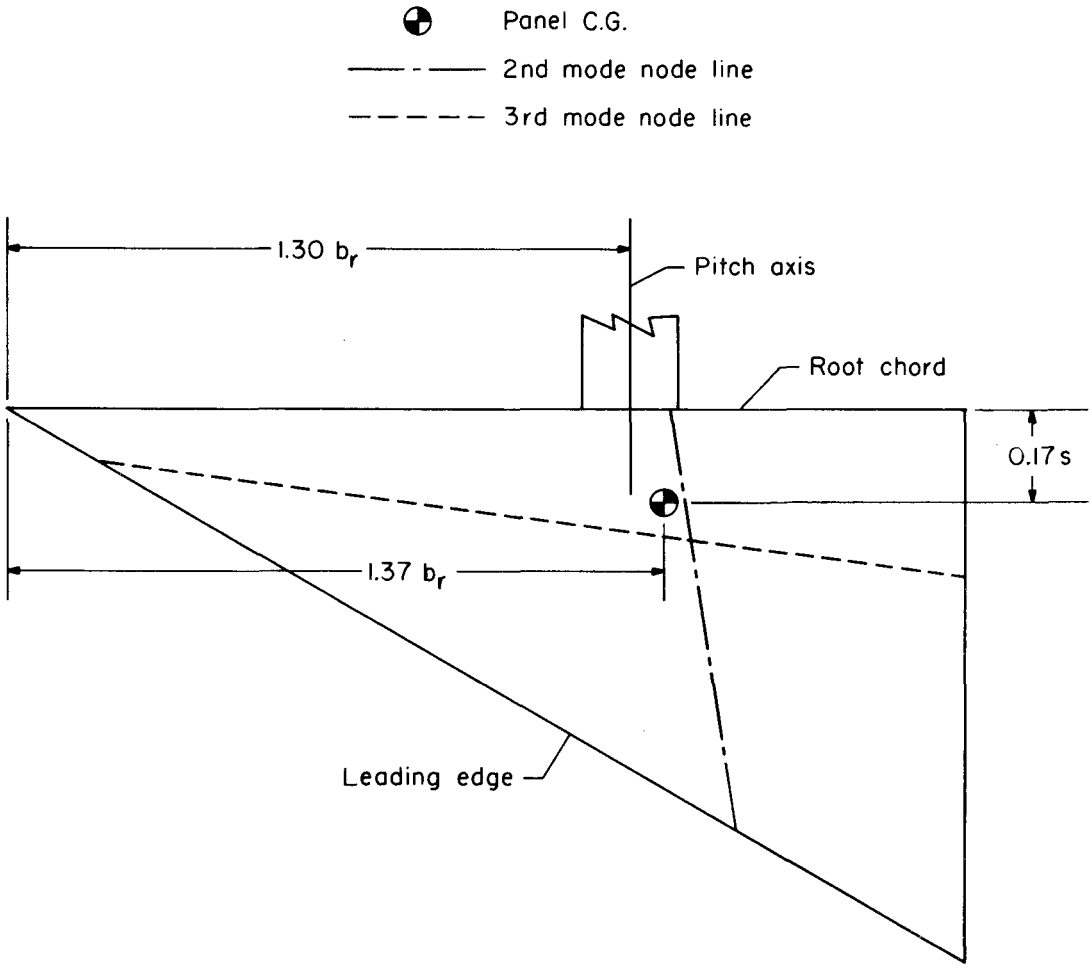

Figure 4.- Typical nodal lines for models; model 60-S-1. (See table I(a) for explanation of model designations.)

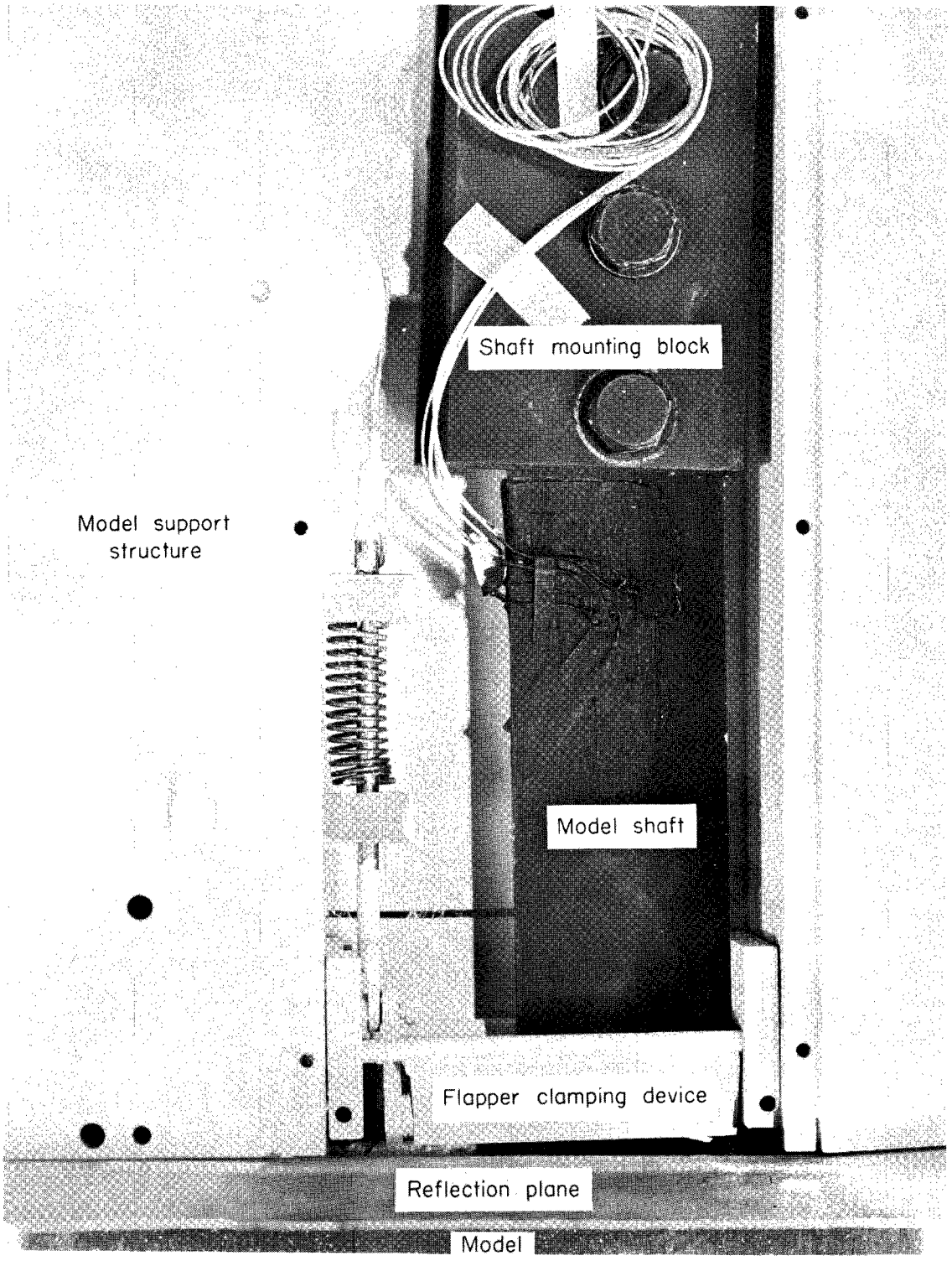

Figure 5.- Clamping apparatus. L-62-3322.1

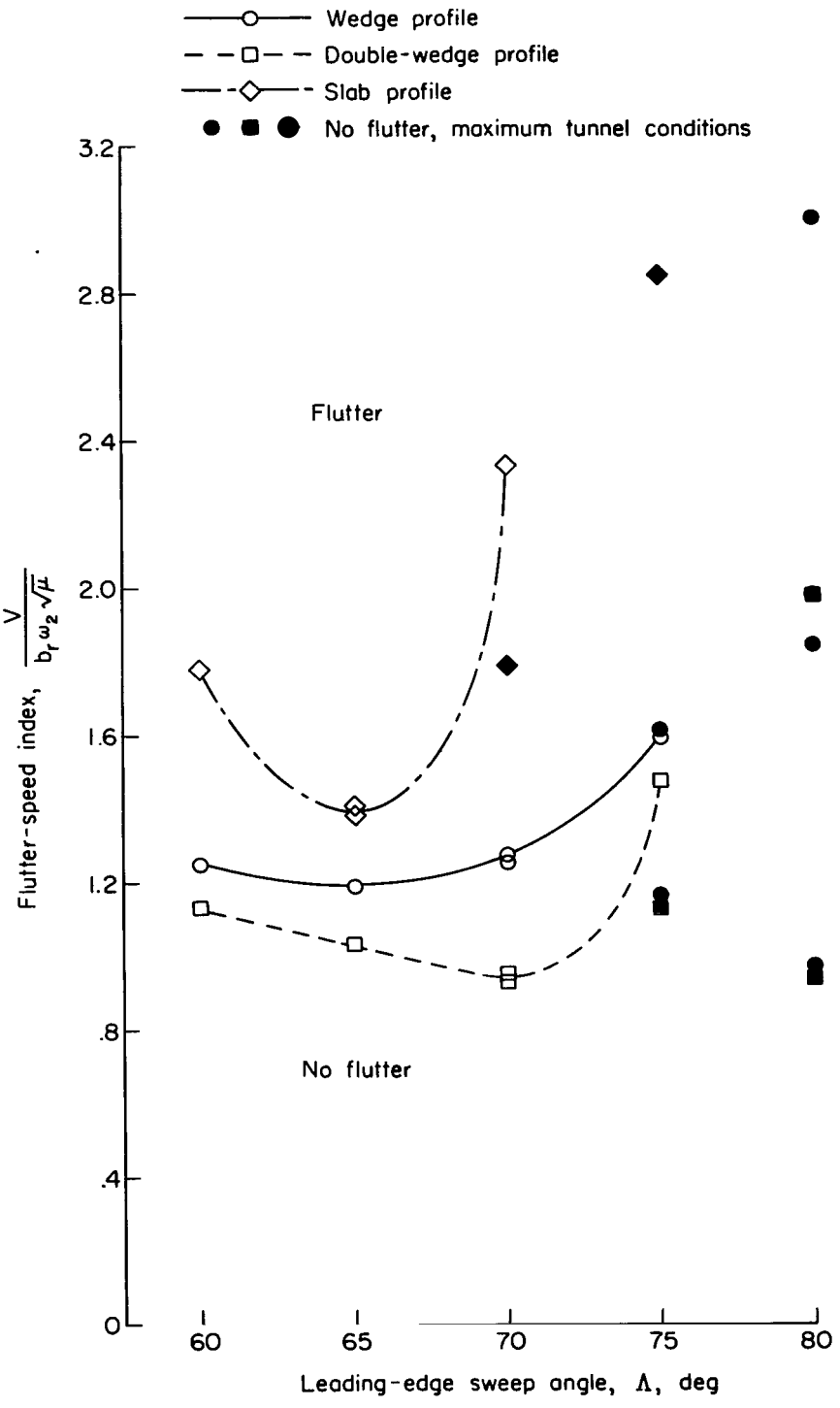

Figure 6.- Variation of flutter-speed index with leading-edge-sweep angle.

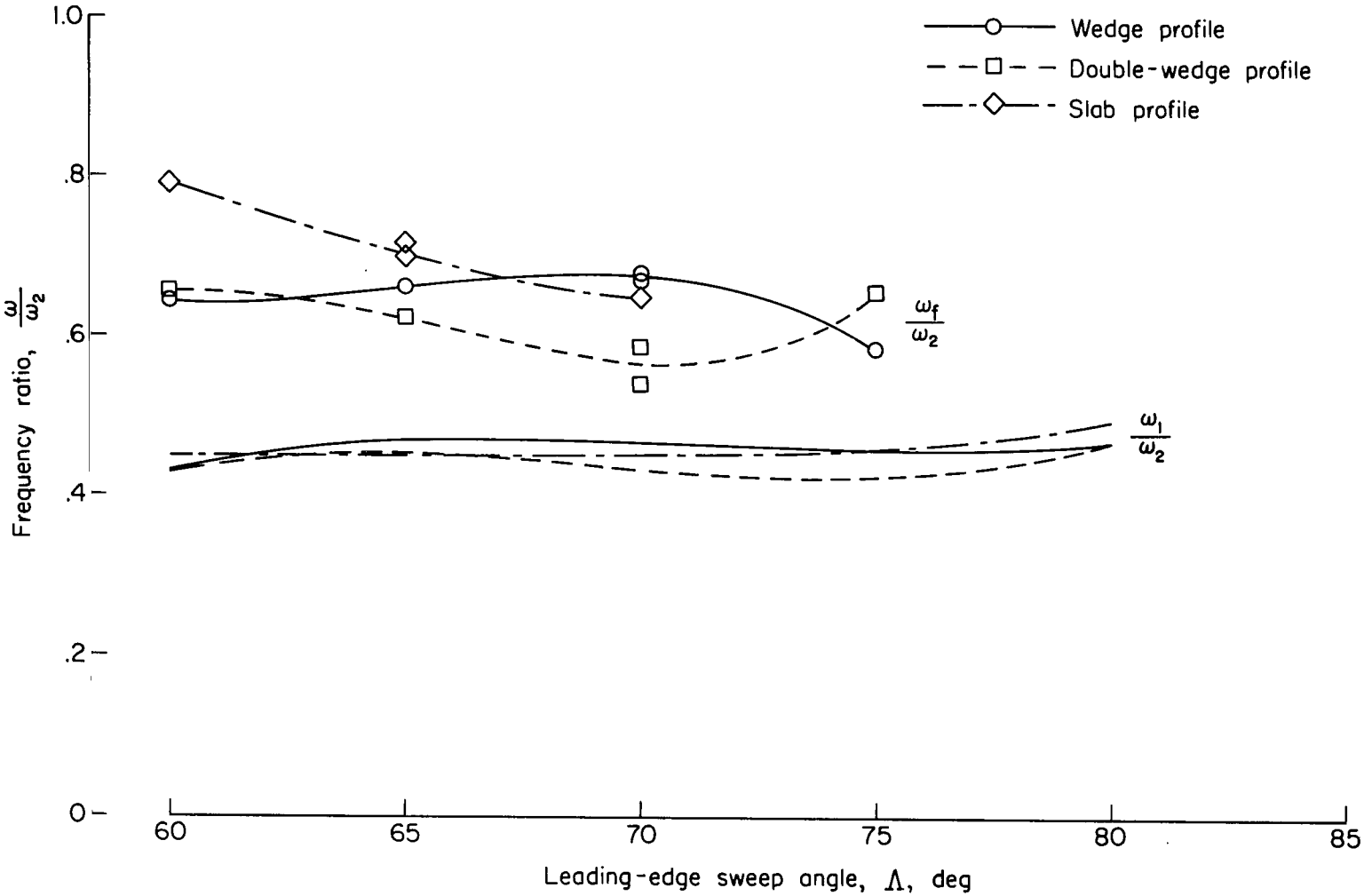

Figure 7.- Variation of frequency ratio with leading-edge-sweep angle.

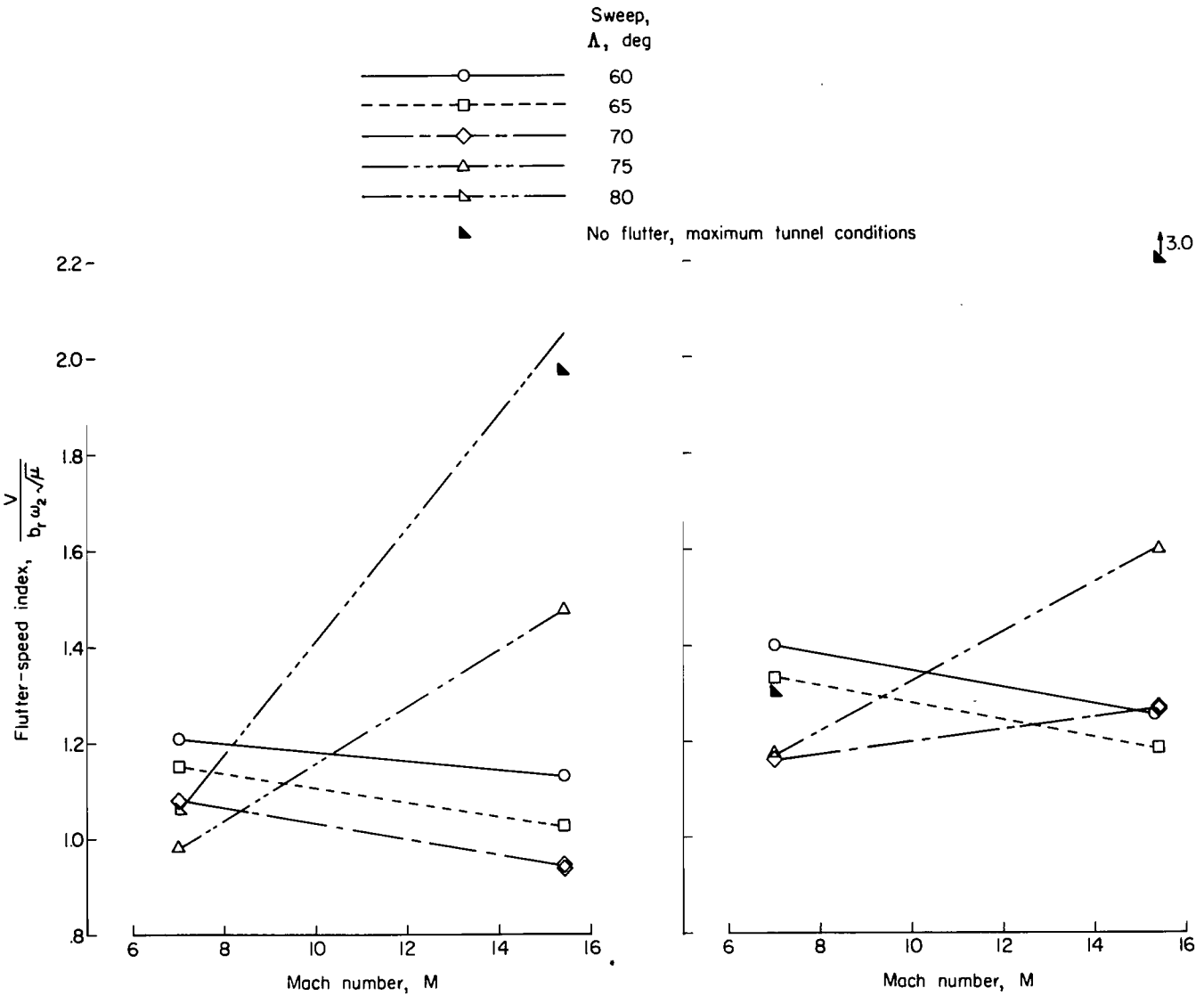

(a) Double-wedge profile, $\bar{x}_o = 0.65$.

(b) Wedge profile, $\bar{x}_o = 0.65$.

Figure 8.- Variation of flutter-speed index with Mach number.

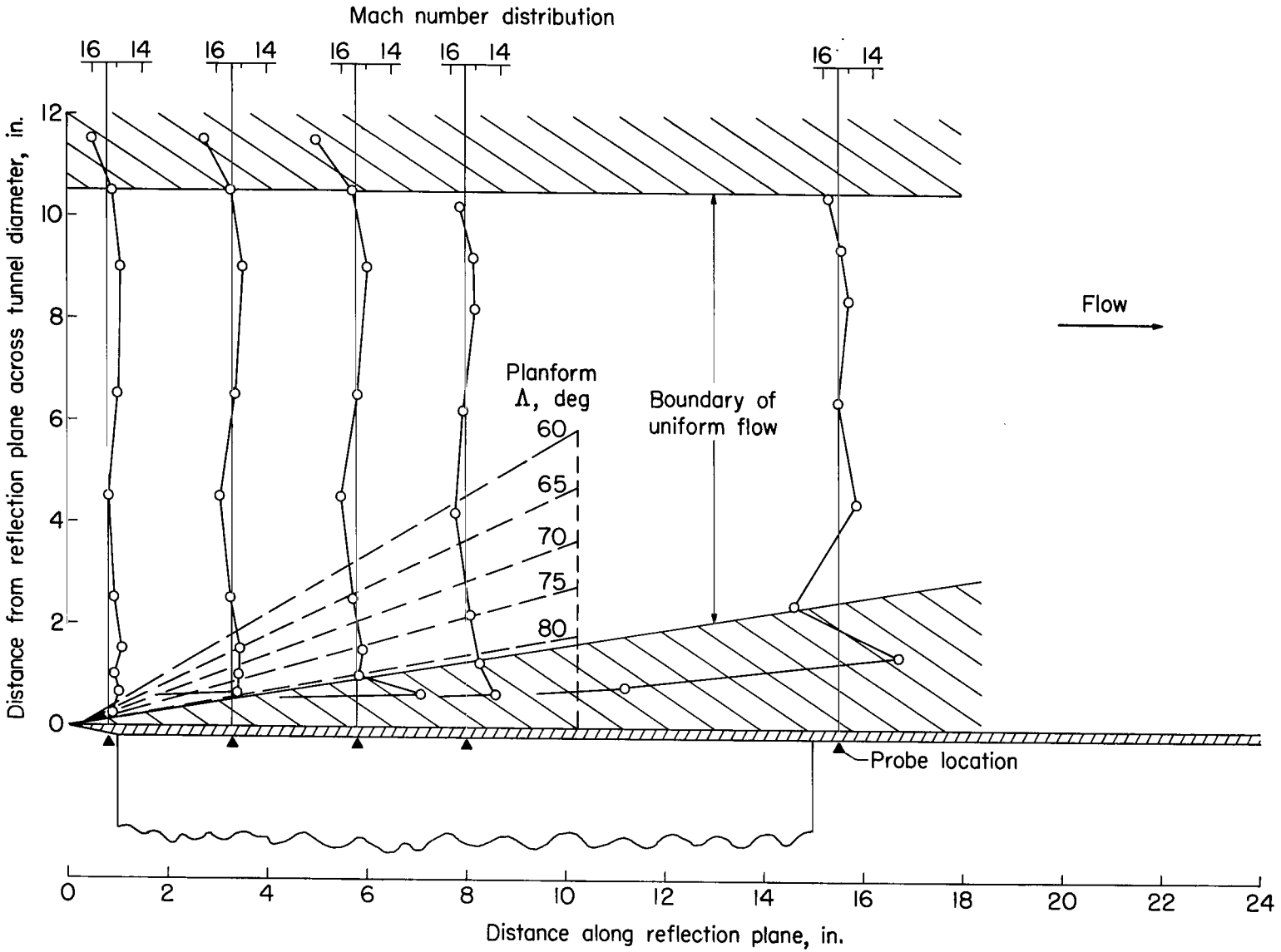

Figure 9.- Mach number survey in the plane of the model. Stagnation pressure = 750 psi (reproduced from ref. 3).

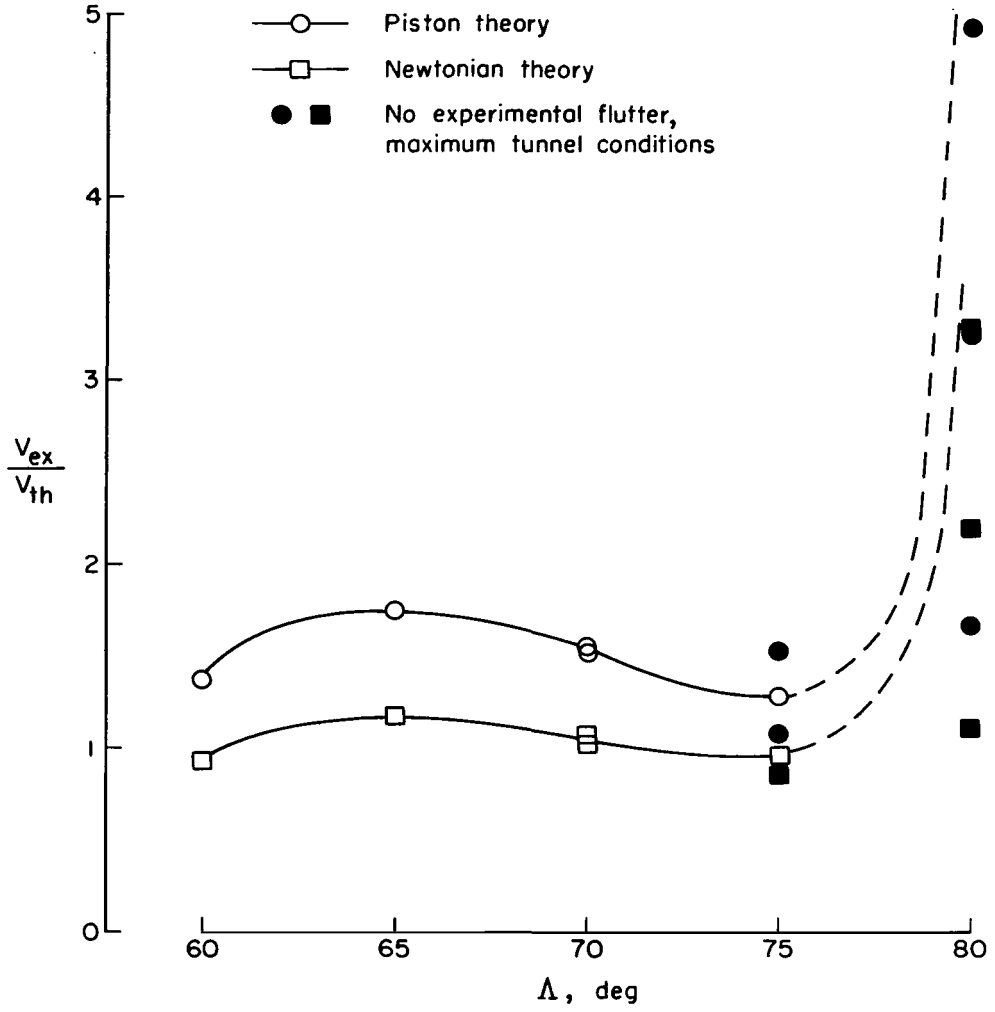

(a) Wedge profile.

Figure 10.- Ratio of experimental to calculated flutter velocity as a function of leading-edge-sweep angle.

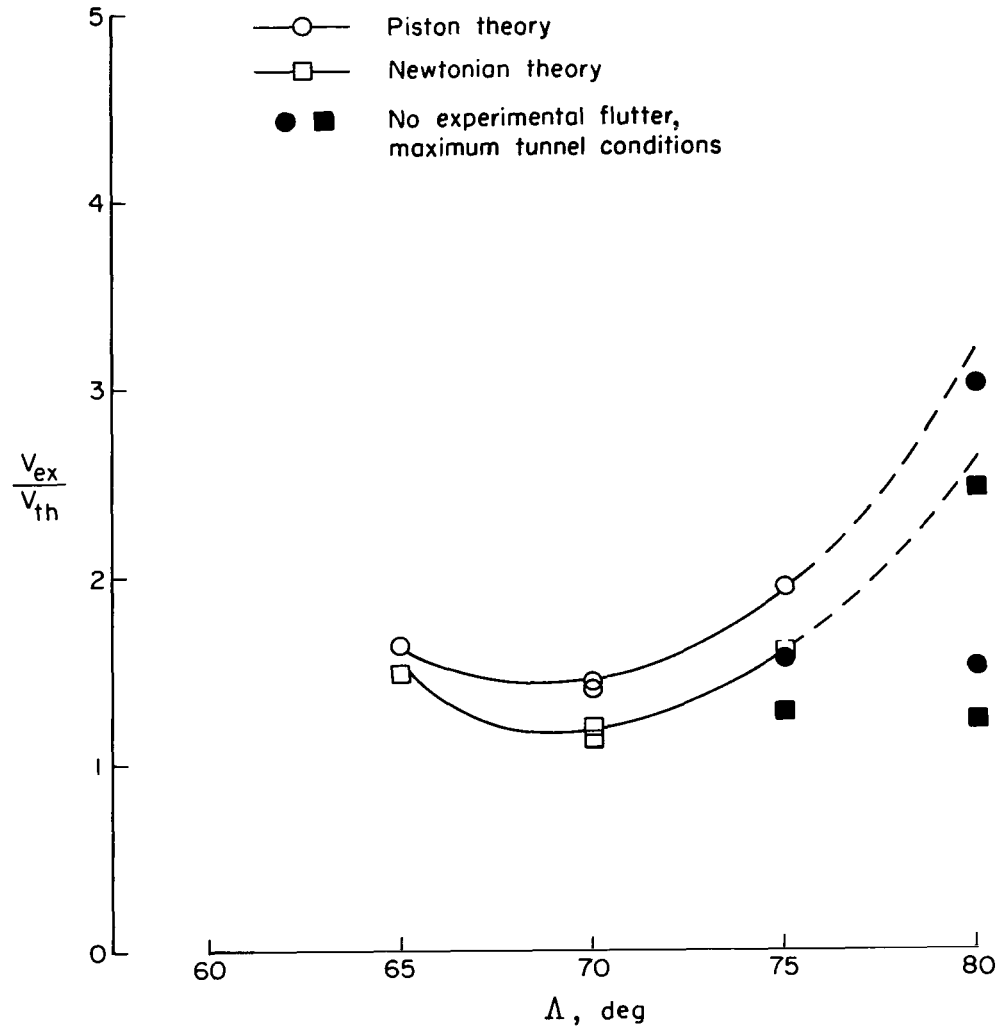

(b) Double-wedge profile.

Figure 10.- Continued.

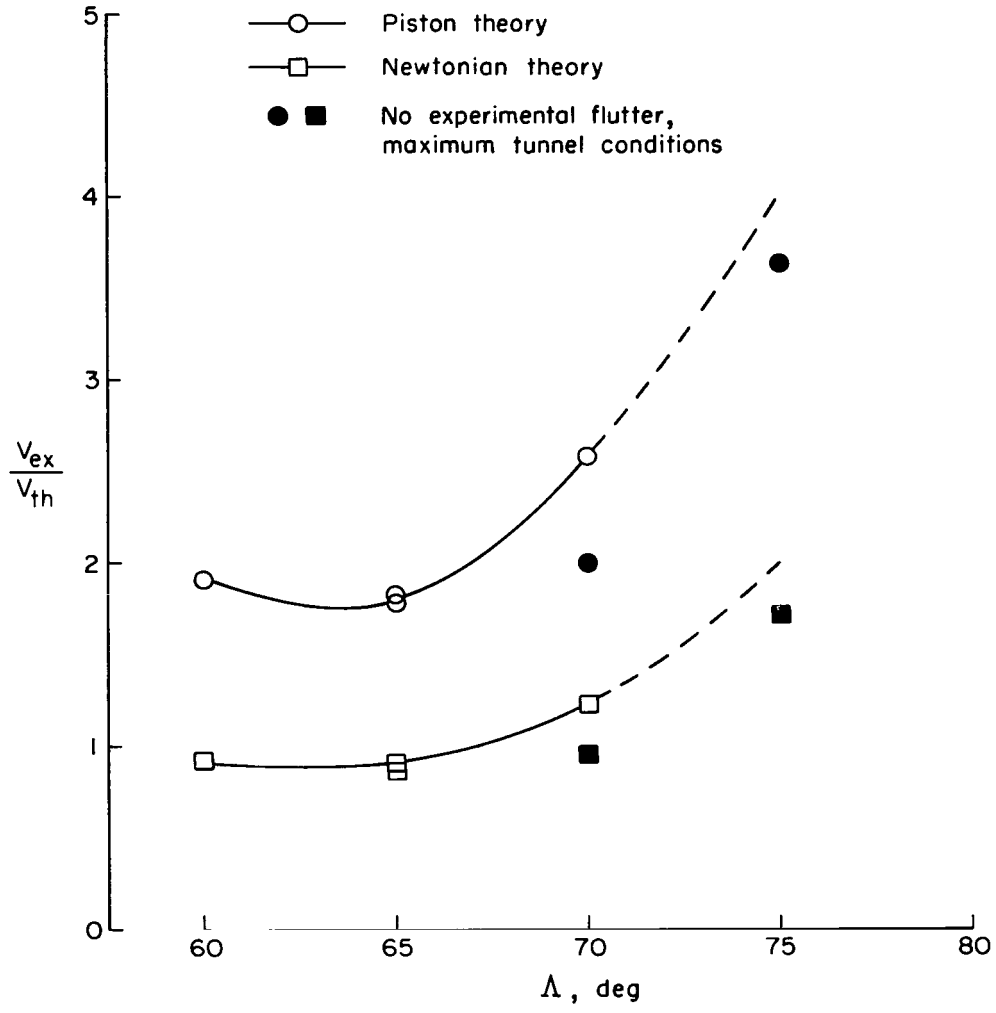

(c) Slab profile.

Figure 10.- Concluded.

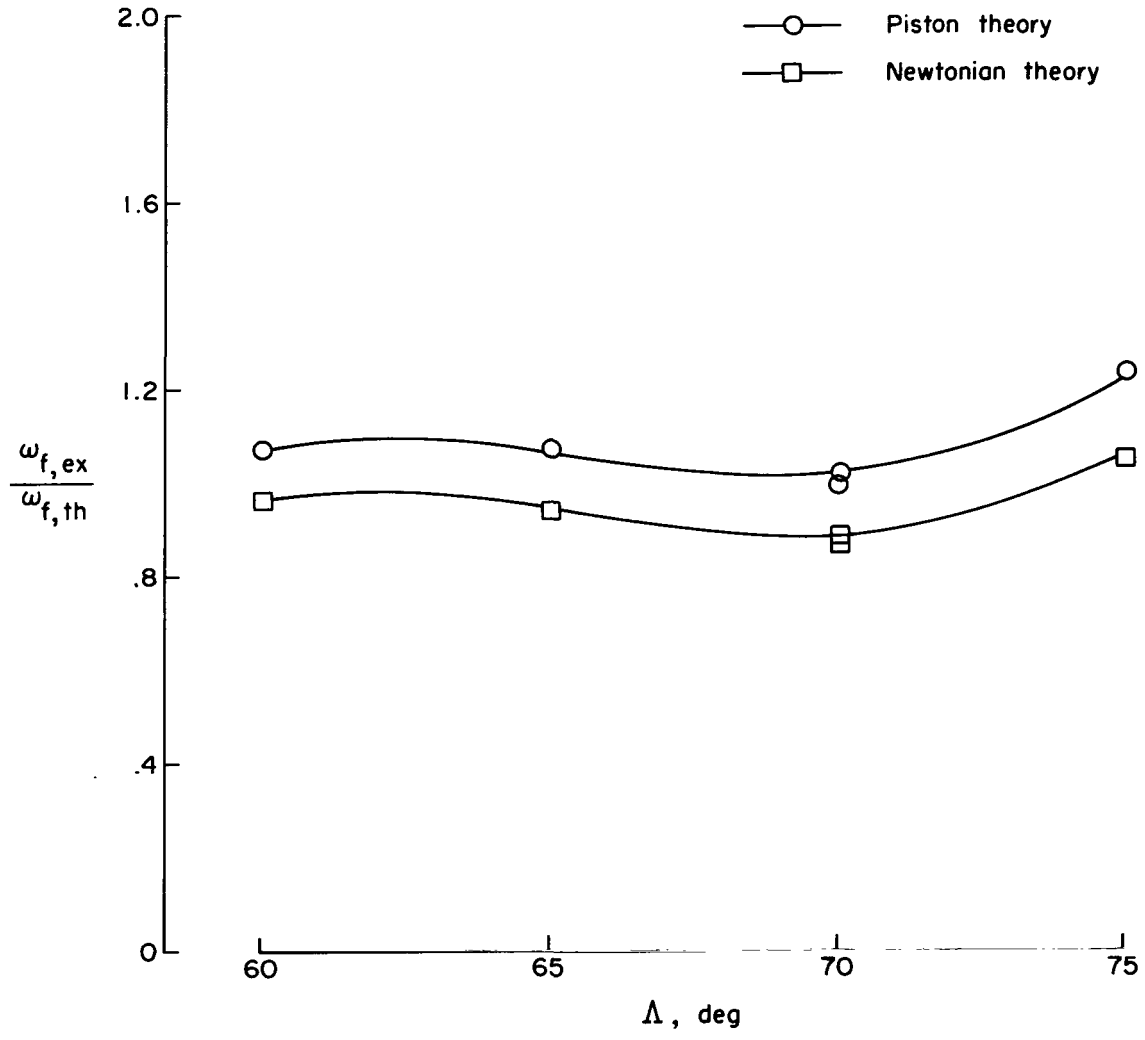

(a) Wedge profile.

Figure 11.- Ratio of experimental to calculated flutter frequency as a function of leading-edge-sweep angle.

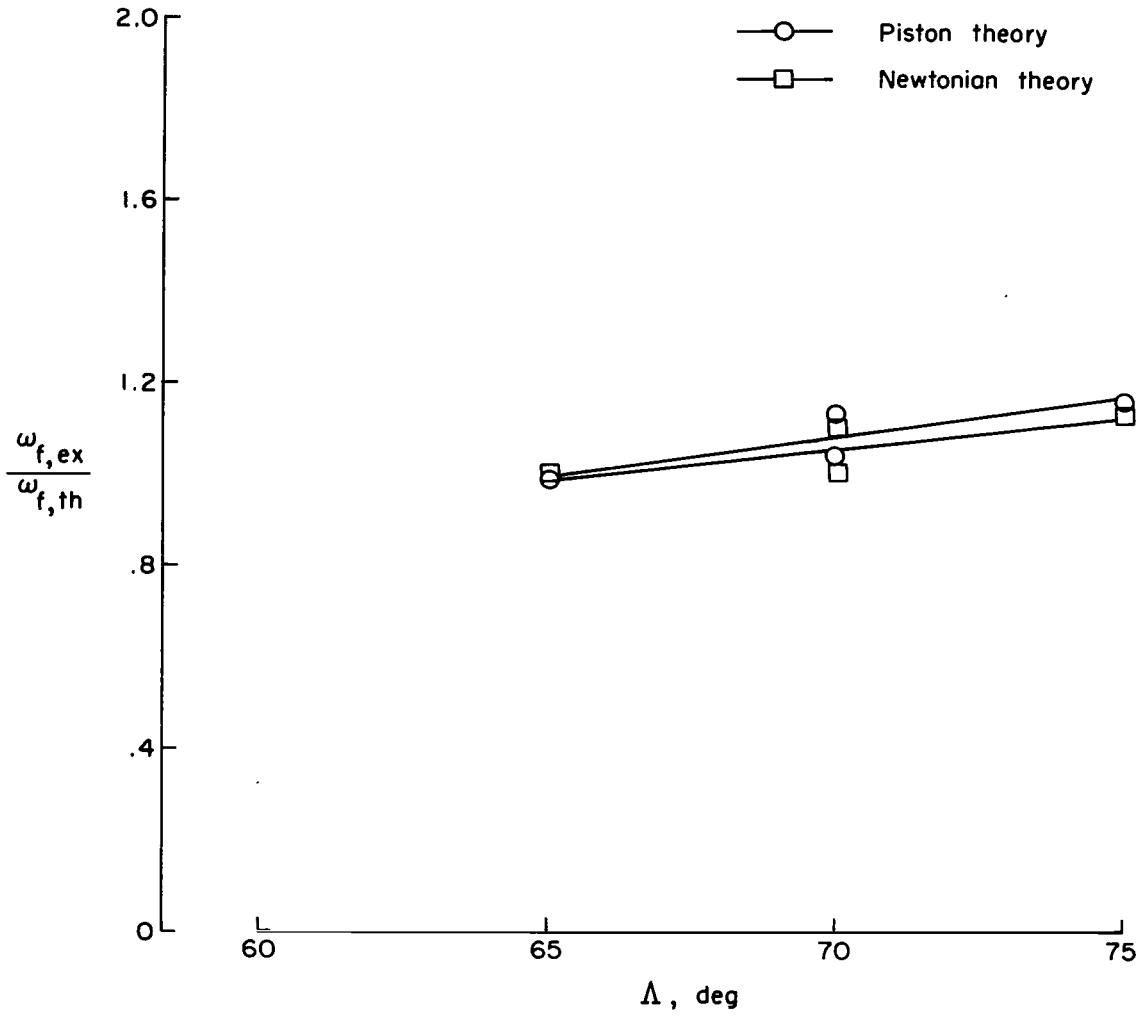

(b) Double-wedge profile.

Figure 11.- Continued.

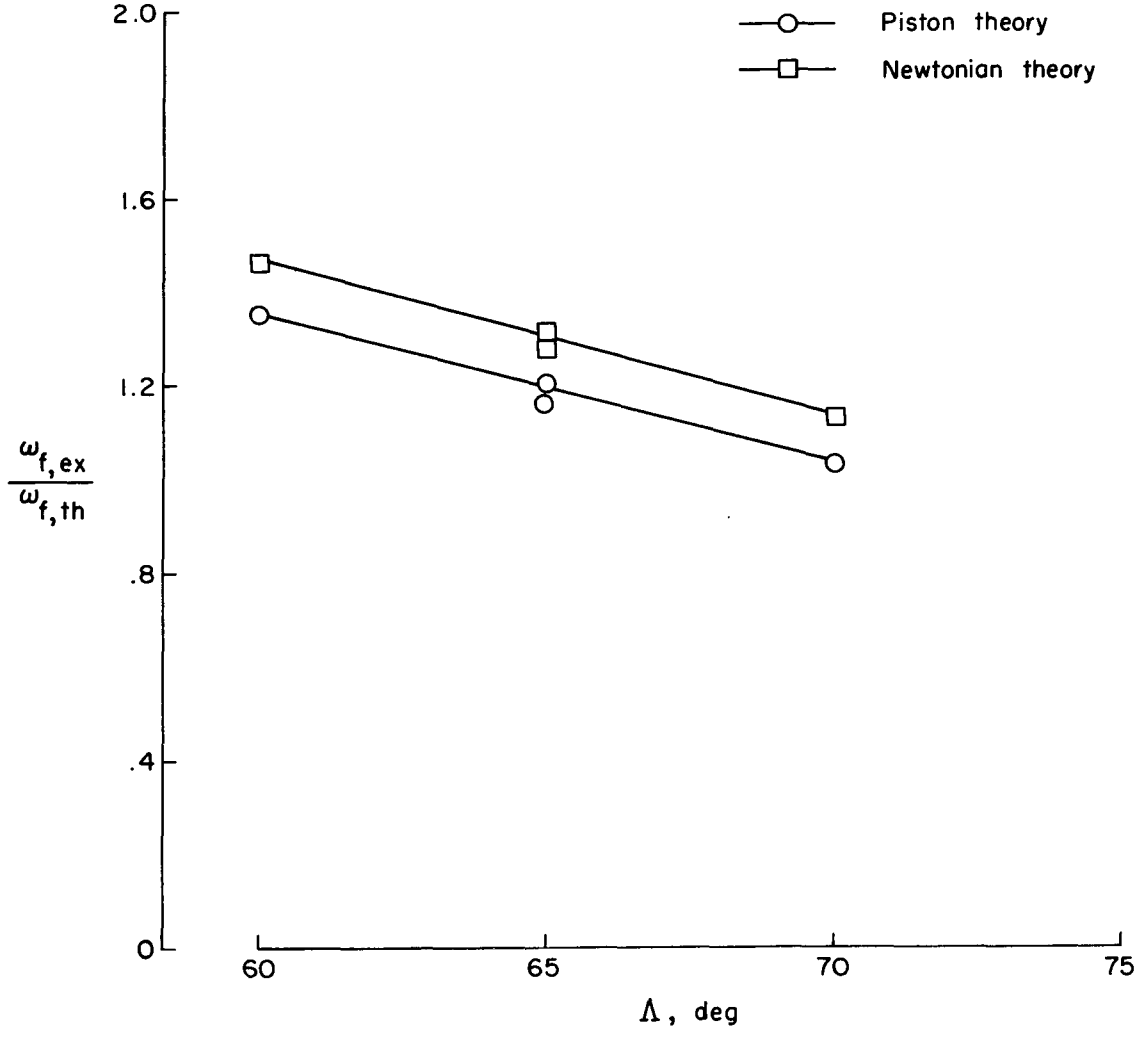

(c) Slab profile.

Figure 11.- Concluded.

2/17/85

"The aeronautical and space activities of the United States shall be conducted so as to contribute . . . to the expansion of human knowledge of phenomena in the atmosphere and space. The Administration shall provide for the widest practicable and appropriate dissemination of information concerning its activities and the results thereof."

—NATIONAL AERONAUTICS AND SPACE ACT OF 1958

NASA SCIENTIFIC AND TECHNICAL PUBLICATIONS

TECHNICAL REPORTS: Scientific and technical information considered important, complete, and a lasting contribution to existing knowledge.

TECHNICAL NOTES: Information less broad in scope but nevertheless of importance as a contribution to existing knowledge.

TECHNICAL MEMORANDUMS: Information receiving limited distribution because of preliminary data, security classification, or other reasons.

CONTRACTOR REPORTS: Technical information generated in connection with a NASA contract or grant and released under NASA auspices.

TECHNICAL TRANSLATIONS: Information published in a foreign language considered to merit NASA distribution in English.

TECHNICAL REPRINTS: Information derived from NASA activities and initially published in the form of journal articles.

SPECIAL PUBLICATIONS: Information derived from or of value to NASA activities but not necessarily reporting the results of individual NASA-programmed scientific efforts. Publications include conference proceedings, monographs, data compilations, handbooks, sourcebooks, and special bibliographies.

Details on the availability of these publications may be obtained from:

SCIENTIFIC AND TECHNICAL INFORMATION DIVISION

NATIONAL AERONAUTICS AND SPACE ADMINISTRATION

Washington, D.C. 20546